Integral equation theory of thermodynamics, pair structure, and growing static length scale in metastable hard sphere and Weeks-Chandler-Andersen fluids

Yuxing Zhou [1], Baicheng Mei [1], and Kenneth S. Schweizer [1,2,*]

[1] *Department of Material Science and Materials Research Laboratory, University of Illinois at Urbana-Champaign, Urbana, Illinois 61801, USA*

[2] *Department of Chemistry and Department of Chemical & Biomolecular Engineering, University of Illinois at Urbana-Champaign, Urbana, Illinois 61801, USA*

(Received 26 January 2020; revised manuscript received 7 March 2020; accepted 24 March 2020; published 20 April 2020)

We employ the Ornstein-Zernike integral equation theory with the Percus-Yevick (PY) and modified-Verlet (MV) closures to study the equilibrium structural and thermodynamic properties of metastable monodisperse hard sphere and continuous repulsion Weeks-Chandler-Andersen (WCA) fluids under density and temperature conditions where the system is strongly overcompressed or supercooled, respectively. The theoretical results are compared to crystal-avoiding simulations of these dense monodisperse model one-component fluids. The equation of state (EOS) and dimensionless compressibility are computed using both the virial and compressibility routes. For hard spheres, the MV-based virial route EOS and dimensionless compressibility are in very good agreement with simulation for all packing fractions, much better than the PY analogs. The corresponding MV-based predictions for the static structure factor are also very good. The amplitude of density fluctuations on the local cage scale and in the long wavelength limit, and three technically different measures of the density correlation length, are studied with both closures. All five properties grow in a roughly exponential manner with density in the metastable regime up to packing fractions of 58% with no sign of saturation. The MV-based results are in good agreement with our crystal-avoiding simulations. Interestingly, the density dependences of long and short wavelength quantities are closely related. The MV-based theory is also quite accurate for the thermodynamics and structure of supercooled monodisperse WCA fluids. Overall our findings are also relevant as critical input to microscopic theories that relate the equilibrium pair correlation function or static structure factor to dynamical constraints, barriers, and activated relaxation in glass-forming liquids.

DOI: 10.1103/PhysRevE.101.042121

I. INTRODUCTION

The one-parameter hard sphere (HS) fluid is the most foundational, generic, and minimalist model of strongly interacting liquid matter [1,2]. Understanding its structure, dynamics, and crystallization has been of interest for half a century. It continues to be relevant either literally or as a reference system for various thermal liquid and soft matter systems, including for questions of structure, glassy dynamics, and kinetic vitrification at ultrahigh packing fractions in the metastable to crystallization regime [2–6]. Reasonably accurate statistical mechanical theories for the pair structure and thermodynamics of equilibrium hard sphere fluids have long existed based on the Ornstein-Zernike (OZ) integral equation and an approximate closure [e.g., Percus-Yevick (PY)] [1,2,7]. However, the facile crystallization of monodisperse spheres has largely precluded testing such theories in the high packing fraction metastable regime relevant to strongly activated glassy dynamics. Indeed, to access the latter has typically required introducing polydispersity, i.e., quenched disorder of particle diameter, or the use of binary mixtures, both of which significantly complicate understanding the basic physics [8–11].

Recently, Zhou and Milner [12,13] have developed a crystal-avoiding simulation method that allows very high packing fraction equilibrated metastable fluid states of monodisperse hard and soft repulsive spheres to be determined. In this article we employ this method to perform simulations which are of interest in their own right and serve as benchmarks to test theories. This is especially relevant to microscopic theoretical approaches that connect slow dynamics with structural correlations, e.g., ideal mode coupling theory (MCT) [14], nonlinear Langevin equation (NLE) theory [15], elastically collective nonlinear Langevin equation (ECNLE) theory [6,16], and thermodynamic approaches to glass formation based on configurational entropy such as the random first order transition theory and its variants [17–19]. Most of these theories require accurate pair structural information as input at very high packing fractions, the regime where integral equation theories (e.g., OZ-PY) are most inaccurate and thermodynamically inconsistent [1,2]. This limitation also impacts making theoretical progress on the question of whether a growing static length defined at the pair correlation level and/or a thermodynamic property does or does not correlate with ultraslow dynamics.

The above discussion provides our motivation to carry out equilibrated monodisperse fluid simulations and revisit OZ theory in search of a better closure relation in the metastable

*kschweiz@illinois.edu

regime of monodisperse hard spheres. We also use the simulation and theoretical results to provide insights concerning the physics of ultradense highly correlated fluids. Concerning our theoretical aspect, we consider the modified-Verlet (MV) closure [20–23]. It was shown long ago [20,21] to produce very accurate results for pair structure and thermodynamic properties of monodisperse hard spheres in the "normal" liquid regime below the crystallization packing fraction of $\phi \sim 0.495$ where glassy dynamics has not yet emerged. The predictions of OZ-MV theory in the metastable regime have, for the most part, not been determined nor confronted with monodisperse hard sphere fluid simulations. One exception is the recent work of two of us which employed MV integral equation theory to compute the equation of state which was compared to crystal-avoiding simulations in the metastable regime [24]. Excellent agreement between the OZ-MV virial route results and simulation was found up to a packing fraction of 0.58. However, the real purpose of Ref. [24] was to study highly size-asymmetric hard sphere mixtures at relatively high temperatures and low densities in the normal fluid regime. This involves very different physics than in the ultrahigh density one-component hard sphere fluid. Neither simulation nor OZ theory studies of other thermodynamic properties, the static structure factor, or real- and Fourier-space correlation lengths were performed. Addressing these issues is the primary purpose of the present article.

We theoretically focus on the high metastable packing fraction regime of $\phi \sim 0.5$ to 0.6, which is still well below the random close packing (RCP) or jamming limit [25]. The upper limit of the latter range corresponds in the ECNLE theory of viscous thermal liquids [6,16] to the laboratory kinetic vitrification point, which exceeds the packing fraction that can typically be equilibrated in colloidal suspension experiments [9]. We also present a combined theory and simulation study of several metastable supercooled states of the continuous repulsive interaction Weeks-Chandler-Andersen (WCA) [26] monodisperse fluid. Our highly limited prior work [24] for this system was in the normal liquid regime at much higher temperatures and lower densities.

Our results from the present study are relevant to constructing more accurate theories of the equilibrium behavior of ultradense hard sphere fluids, density functional theories of crystallization [27] and interfaces [28], phase separation of hard sphere mixtures [29,30] and polymer-colloid mixtures [31,32], etc., but our prime motivation is its relevance as input to the dynamical theories mentioned above, which to date have most often used the PY closure [10,14,33–35]. Extant microscopic theories of glassy dynamics typically require to high accuracy the Fourier-space static structure factor, $S(q)$, or the direct correlation function, $C(q)$, including at very large wave vectors not easy to accurately determine with simulation. For the ideal MCT of the hard sphere fluid [14], use of a more accurate structural theory will have little consequence since the (unphysical) critical power law divergence of the relaxation time occurs at $\phi_c \sim 0.515$ where errors incurred by PY theory are rather modest. In strong contrast, NLE and ECNLE theories that include activated hopping [6,15,16] do not have any dynamical divergences below RCP, and make predictions for values of ϕ well beyond 0.515 which may be sensitive to including improved structural input.

In addition to studying the pair correlation function in real, $g(r)$, and Fourier, $S(q)$, space and thermodynamic properties, we also analyze how correlation lengths and density fluctuation order parameters evolve with packing fraction. The nature of growing static length scales defined at the pair level and their possible correlation with activated glassy dynamics has been an enduring question. A rather common presumption in the literature is that such length scales vary little with thermodynamic state in glass-forming liquids and/or such information is not adequate to understand strongly activated relaxation. We believe these notions are likely not valid, a view supported by the recent successes of ECNLE theory of strongly activated dynamics [6,16,36,37] and machine learning simulation [38,39] studies.

In Sec. II we briefly review OZ theory, the closures studied, and the crystal-avoiding simulation method employed. Section III presents our core theoretical results for the metastable hard sphere fluid, quantitatively compares them to simulation, and deduces inter-relations. A sample result is shown for the implications of using better structural input to the ECNLE theory of activated glassy dynamics. Equilibrium structural and thermodynamic results for the metastable WCA fluid are presented in Sec. IV. The paper concludes with a summary and discussion in Sec. V.

II. THEORY AND SIMULATION METHODS

A. Integral equation theories

The radial distribution or pair correlation function, $g(r)$, obeys the OZ equation [1]:

$$h(r) = c(r) + \rho \int c(|\vec{r} - \vec{r}'|)h(r')d\vec{r}', \tag{1}$$

where ρ is the particle number density, $h(r) \equiv g(r) - 1$, and Eq. (1) defines the direct correlation function $c(r)$. It is convenient to introduce the "cavity distribution function": $y(r) = e^{\beta u(r)}g(r)$, where $u(r)$ is the pair potential and β is the inverse thermal energy. The PY approximation for a general pair potential, $u(r)$, can then be expressed as [1]

$$c(r) = g(r) - y(r) = [e^{-\beta u(r)} - 1]y(r) \equiv f(r)y(r), \tag{2}$$

where $\beta \equiv (k_B T)^{-1}$ is the inverse thermal energy. For hard spheres of diameter σ, this corresponds to $c(r) = 0, \ r > \sigma$. The MV closure can be viewed as interpolating between the PY and hypernetted chain (HNC) closures in γ-space [20], where $\gamma(r) \equiv h(r) - c(r)$. Specifically, one can generically write the pair correlation function as

$$g(r) = \exp[-\beta u(r) + \gamma(r) + b(r)], \tag{3}$$

where if the bridge function, $b(r)$, is exactly known then Eq. (3) is exact. In the MV closure approximation one has

$$b^{\mathrm{MV}}(r) = -\frac{a_1\gamma^2(r)}{1 + a_2|\gamma(r)|}. \tag{4}$$

For hard spheres $a_1 = 1/2$ and $a_2 = 4/5$ were used in the original work [20] in order to *exactly* reproduce the fourth virial coefficient while improving the fifth virial coefficient

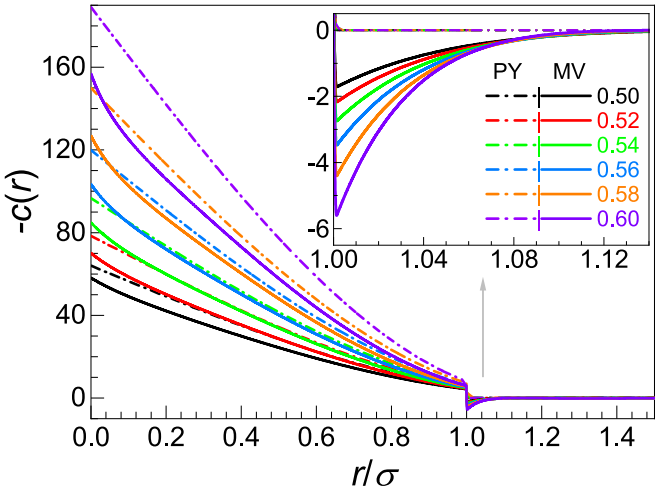

FIG. 1. Direct correlation function for packing fraction ϕ from 0.5 to 0.6 (bottom to top) based on PY (dash-dotted) and MV (solid) closures. Inset is an expanded view of the near contact region.

compared to its PY value. The absolute value of γ enters the denominator in Eq. (4) to avoid the singularity at $\gamma = -1/a_2$, which also assures that the first and second derivatives of Eq. (4) with respect to γ are continuous [22]. We explore the predictions of the PY- and MV-based theories in the high packing fraction regime $\phi = 0.5$ to 0.6. We also consider the WCA fluid at reduced densities and temperatures in the modestly supercooled regime accessible to simulation with the *same* nonoptimized parameters a_1 and a_2 employed for hard spheres.

The negative of $c(r)$ in units of thermal energy plays the role of a renormalized pair potential [1]. Figure 1 presents numerical calculations of this quantity in the high density regime. One sees significant differences between the PY and MV results, with the absolute value of $c(r)$ from PY larger than its MV analog inside the hard core. Outside the hard core the PY direct correlation function incorrectly vanishes, while the MV predicts (inset) a short-range negative tail (an effective attraction) which grows strongly with increasing density, features in qualitative accord with the exact $c(r)$ [1,2,40]. The exact $c(r)$ is also known [41,42] to weakly oscillate outside the hard core. If one blows up the inset in Fig. 1 we do find (not shown) oscillatory behavior with an amplitude that grows with density. However, the oscillations are not about zero since in the MV approximation (and also for HNC) the direct correlation function is strictly non-negative.

B. Simulations

We employ the recently developed crystal-avoiding method [12,13] to simulate monodisperse HS and WCA equilibrium fluids. All simulation results presented in this article are different from our previous results, except for the hard sphere equation-of-state data [24].

Briefly, the crystal-avoiding simulations are based on a hybrid Monte Carlo method, a short molecular dynamics (MD) trajectory from a given amorphous configuration is first generated, and then the difference in crystallinity is measured using a bond-order parameter and the trajectory is accepted or rejected using the Metropolis algorithm. If the move is rejected, all particle velocities are randomized from a Maxwell-Boltzmann distribution before the next trial. This method essentially samples trajectories in phase space for which crystallization did not occur. For hard spheres, event-driven MD is used for generating short trajectories, while for WCA fluids the standard leapfrog integration method is employed. All technical details can be found in Refs. [12,13].

III. HARD SPHERE FLUID RESULTS

A. Equation of state

As relevant background we recall our recent results [24] for the hard sphere fluid equation of state (EOS) using two formally exact statistical mechanical routes which emphasize either the most local part of $g(r)$ (virial route) or the long wavelength integrated aspect (compressibility route). In the former, the reduced pressure is directly related to the contact value, $g(\sigma)$, as [1,43]

$$\frac{\beta P}{\rho} = 1 + \frac{2\pi\rho\sigma^3 g(\sigma)}{3}. \tag{5}$$

The compressibility route is based on the isothermal compressibility, $\kappa_T = -V^{-1}(\frac{\partial V}{\partial P})_T$, and its dimensionless analog $S_0 = S(q=0)$ defined as [1,43]

$$S_0 = \rho k_B T \kappa_T = 1 + \rho h(q=0). \tag{6}$$

The connection to thermodynamics is

$$S_0^{-1} = \frac{\partial \beta P}{\partial \rho}. \tag{7}$$

The reduced pressure follows via integration yielding the compressibility route EOS:

$$\frac{\beta P}{\rho} = \frac{1}{\rho}\int_0^\rho d\rho' \frac{1}{S_0(\rho')}. \tag{8}$$

Figure 2 shows theoretical results [24] using the virial (v) and compressibility (c) routes. For comparison, the empirical Carnahan-Starling (CS) formula as a function of packing fraction $\phi = \pi\rho\sigma^3/6$ [40] is given by

$$\beta P/\rho \approx (1+\phi+\phi^2-\phi^3)/(1-\phi)^3, \tag{9}$$

which is also plotted, along with our simulation results [24] which now include a single (highest shown) packing fraction nonequilibrium data point. The simulations agree well with the CS formula for $\phi < 0.545$, but not beyond. The PY virial and compressibility route results differ significantly, with PY(v) strongly underestimating pressure, while PY(c) agrees much better with simulation. In contrast, the MV results are more thermodynamically consistent, with the virial route results in good accord with simulation for all packing fractions; only at the single highest equilibrated packing fraction (0.585) simulated can one see deviations. Thus, MV theory is accurate for the EOS, and also its derivative with density of the reduced pressure which is an important property per Eq. (7).

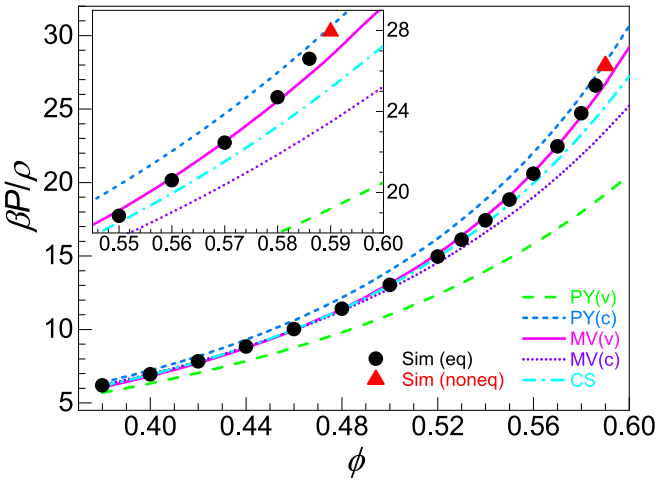

FIG. 2. Dimensionless equation of state for various theoretical calculations and our hard sphere crystal-avoiding simulation data [24]. The green (long-dashed), blue (dashed), magenta (solid), purple (dotted), and cyan (dash-dotted) curves indicate results for PY virial, PY compressibility, MV virial, MV compressibility, and CS approximations, respectively. The black circle and red triangle data are from the simulations under equilibrium [24] and nonequilibrium conditions, respectively. Inset: expanded view of the same results for high packing fractions (0.55–0.60).

We note in passing that Ref. [11] found that a polydisperse version of the CS formula works well up to packing fractions of ∼63%. However, this study employed an extremely polydisperse hard sphere model, which is not relevant to our present work.

B. Pair structure

The contact value of $g(r)$ plays an essential role in determining the thermodynamics and dynamics of hard spheres. Given Eq. (5), one can immediately deduce from Fig. 2 that the high accuracy of the MV(v) reduced pressure implies excellent results for the contact value, significantly superior to those of the PY and CS approaches. Concerning the full $g(r)$, we refrain from showing plots since we find the MV and PY calculations are both very accurate beyond the separation that defines the first minimum of $g(r)$. At smaller distances, the MV results are much better and in good agreement with our simulations.

Due to its relevance to scattering experiments and central role in dynamical theories [1,14–16,44–47] we consider in detail the Fourier-space static structure factor:

$$S(\vec{q}) = \frac{1}{N}\langle \rho(\vec{q})\rho(-\vec{q})\rangle, \quad \rho(\vec{q}) = \sum_{j=1}^{N} \exp(i\vec{q}\cdot\vec{r}_j), \tag{10}$$

which in our simulations is computed as

$$S(q) = 1 + 4\pi\rho \int_0^\infty dr\, r^2 \frac{\sin(qr)}{qr}[g(r) - 1]. \tag{11}$$

Figure 3 shows our results. In all cases, PY overpredicts the first peak, and is inferior to the MV results. The latter are excellent for this feature except at the highest density where small errors are incurred. As typically observed in $g(r)$ of glass-forming sphere liquids [4,9,48], the second peak of $S(q)$ also "splits" at high densities, which the theories do not capture. However, except for this feature the MV results at higher wave vectors are in excellent accord with simulation, significantly better than PY.

C. Density fluctuation order parameters

The amplitude of the first peak of the structure factor, $S_{\max}$, quantifies the coherence or intensity of short-range amorphous order. The main frame of Fig. 4 plots this quantity as a function of packing fraction. Despite PY theory underpredicting the contact value of $g(r)$, it systematically overpredicts this Fourier-space quantity. In contrast, MV theory is in near perfect agreement with simulation for $S_{\max}$. Interestingly, the inset of Fig. 4 shows that $S_{\max}$ is well described by an exponential form, $A\exp(B\phi)$, for both closures with fit parameters reported in Table I. The parameter B is ∼5.2 and 6.5 for MV and PY, respectively.

Concerning the exponential fits, it is the best two-parameter description of the above (and below) theoretical results we have found. However, we are not arguing for a fundamental significance of this form, and have tested it only over the packing fraction range studied here. At even higher densities we do not expect the exponential form will continue to be accurate since eventually the RCP jammed state is

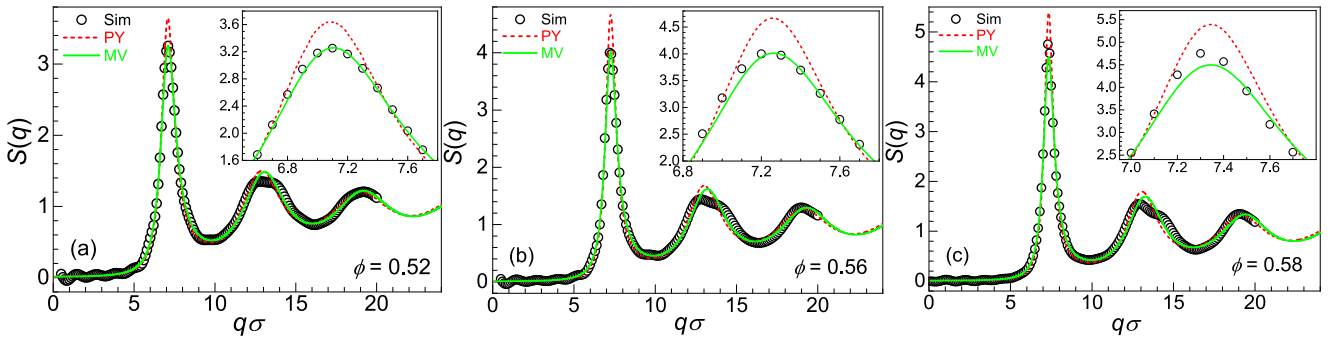

FIG. 3. Static structure factor as a function of dimensionless wave vector for three packing fractions $\phi = 0.52$, 0.56, and 0.58 based on the PY (red dashed lines) and MV (green solid) closures and the crystal-avoiding simulation results (black circles). Insets show an expanded view of the first peak region.

TABLE I. Parameters A and B of the exponential fits, $A\exp(B\phi)$ in Figs. 4–8 for the PY and MV closure theoretical results. Length scales are in units of the hard sphere diameter. From left to right the quantities are as follows: the value of $S(q)$ at its first peak, inverse dimensionless compressibility computed from the $q = 0$ limit of the static structure factor per Eq. (6); inverse dimensionless compressibility computed using the virial route relation of Eq. (7); a Fourier-space derived correlation length extracted from the full width at half maximum, λ, of $S(q)$; a Fourier-space derived correlation length defined in Eq. (14); and the density correlation length extracted from an exponential fit of the envelope of $|rh(r)|$.

		$S_{\max}$	$1/S_0 = 1/S(q=0)$	$1/S_0$ (virial)	$l = \pi/\lambda$	Ψ	ξ_ρ
PY	A	0.0125	0.3097	0.5913	0.1179	0.0534	0.0746
	B	6.535	10.663	8.581	6.107	7.023	6.404
MV	A	0.224	0.543	0.213	0.117	0.0937	0.105
	B	5.200	9.182	11.277	6.056	5.671	5.5152

approached [25], which is not correctly captured by PY- or MV-based OZ theory.

A very different "scalar order parameter" is the dimensionless amplitude of long wavelength density fluctuations, $S(q = 0) = S_0$. Although a thermodynamic property, it is directly related to an integrated measure of nonrandom structure over *all* length scales given, Eq. (6). Moreover, it plays a central role in the predictive mapping employed in ECNLE theory of activated relaxation to treat molecular and polymeric thermal liquids in terms of an effective hard sphere fluid [16,49]. Figure 5 shows PY and MV theory results for this quantity plotted in an inverse representation and log-linear format. Results are shown based on both the direct calculation of $S(q = 0)$ and an indirect route corresponding to differentiation of the virial route EOS using Eq. (7). Both theories are thermodynamically inconsistent, but MV far less so than PY. Interestingly, all theoretical results are again empirically well described by a nearly exponential growth of $1/S_0$ with packing fraction, as indicated by the straight line fits with parameters given in Table I.

Our discrete equation-of-state simulation data of Fig. 2 are fit to interpolating curves and $1/S_0$ extracted using Eq. (7). Results up to packing fractions that this numerical exercise can be accurately carried out are shown in Fig. 5. Compared to these simulation data, both the MV(v) and PY(c) results are quite accurate with $B \sim 11$ in the exponential fit. Interestingly, the numerical results in the metastable regime are generically well captured by an exponential form for both the local and long wavelength order parameters, $S_{\max}$ and S_0, with the value of B for $1/S_0$ roughly double that of $S_{\max}$, and hence $1/S_0 \propto S_{\max}^2$ based on the MV-virial analysis.

D. Real-space density correlation length

We now study the real-space density correlation length. Motivated by the classic idea that $h(r)$ is of a damped oscillatory Yukawa form [1,2,50] characterized by a single decay length (density correlation length) at large enough interparticle separations, Fig. 6 plots MV theory results for $|(r/\sigma)\, h(r)|$ versus r/σ in a log-linear manner over a wide range of high

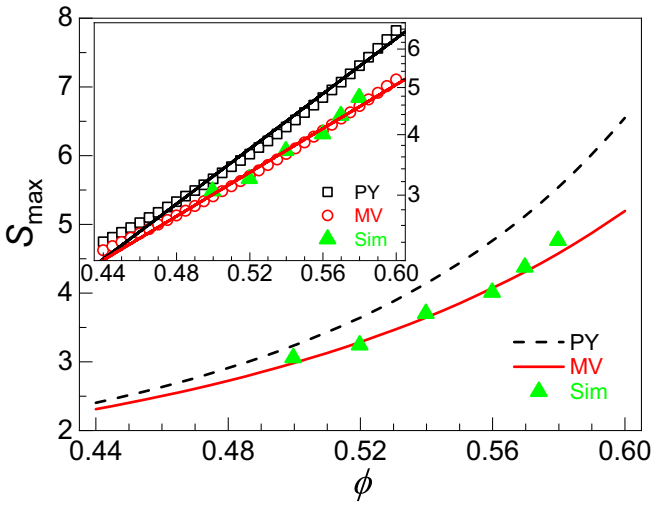

FIG. 4. Value of the first peak of the structure factor as a function of packing fraction for PY (black dashed curve) and MV (red solid curve) closures and our hard sphere simulations (green triangles). Inset shows the same results as the main frame but in a log-linear manner. The straight lines in the inset are exponential fits: $S_{\max} = A\exp(B\phi)$, where the fit parameters are listed in Table I.

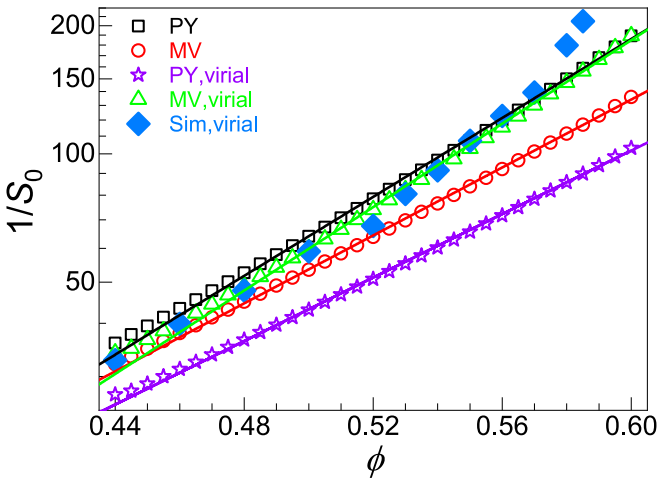

FIG. 5. Inverse dimensionless compressibility computed directly from $S(q = 0)$ as a function of packing fraction for PY (black square) and MV (red circle) closures. Corresponding results based on the virial route of Eq. (7) are shown for PY (purple star) and MV (green triangle) approximations, and our simulation (blue diamond) data. The lines are exponential fits: $S_0^{-1} = A\exp(B\phi)$, where the fit parameters are listed in Table I.

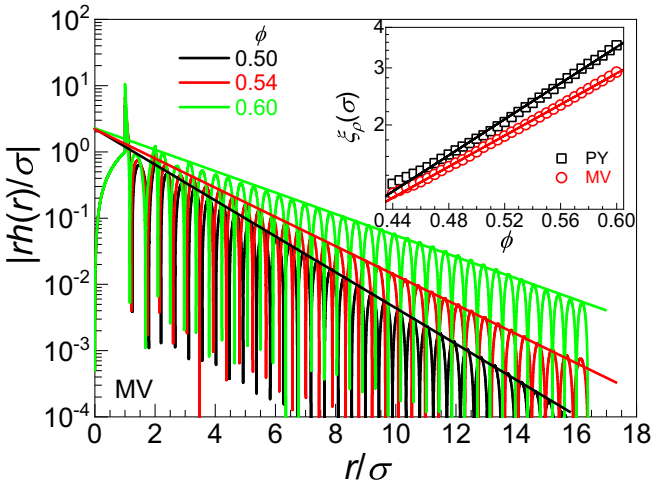

FIG. 6. Main frame: Absolute value of $rh(r)/\sigma$ calculated using OZ-MV theory as a function of normalized radial distance r/σ for three packing fractions. Inset: Packing fraction dependence of the real-space density correlation length (in units of hard sphere diameter) for the PY (black) and MV (red) closures. The lines in the inset are exponential fits: $\xi_\rho = A\exp(B\phi)$, with the fit parameters listed in Table I.

packing fractions. Beyond $r \sim 3{-}4\ \sigma$ the decay envelope is extremely well described by an exponential, $\sim\exp(-r/\xi_\rho)$. Curiously, the lines extrapolate back to a common intersection point at $r = 0$. The inset shows the extracted density correlation length, ξ_ρ, based on PY and MV calculations, which grows from $\sim 1.5\sigma$ at $\phi \sim 0.5$ to $\sim 3\sigma$ at $\phi \sim 0.6$. Both theoretical results follow quite well an exponential growth of ξ_ρ with packing fraction, with $B \sim 5.5$ and 6.4 for MV and PY, respectively.

Figure 7 presents our analogous simulation results in the metastable regime. We follow standard procedure and fit $rh(r)$ from $r \sim 2\sigma{-}6\sigma$ to the analytic form [1,41,42,51]:

$$rh(r) = Ae^{-\alpha_0 r}\cos(\alpha_1\, r - \theta), \tag{12}$$

where $\xi_\rho = 1/\alpha_0$. Figure 7(a) shows the simulation data are very well described by Eq. (12). The main frame of Fig. 7(b) compares our simulation, PY and MV results for the density correlation length. We find the theoretical correlation lengths extracted using Eq. (12) are identical to those obtained from simply fitting the envelope of $\ln|(r/\sigma)\,h(r)|$ in Fig. 6 to an exponential. An important simulation finding is the correlation length continues to grow beyond the equilibrium melting packing fraction $\phi_m = 0.545$, reaching ~ 2.7 particle diameters at $\phi = 0.58$. The MV-based OZ theory agrees well with our simulation data, while the PY approximation predicts a length scale that is too large and grows too strongly with density.

The inset of Fig. 7(b) plots the two key fit parameters in Eq. (12) extracted by analyzing our simulation and theoretical results. This representation is shown to allow comparison with the monodisperse hard sphere fluid simulations of Statt *et al.* [51] who used a standard, not crystal-avoiding, algorithm. We note that the analysis in [51] also employed Eq. (12) and performed fits over the range of $1.5 < r/\sigma < 4$. One sees there is excellent agreement between the two simulation studied up to $\phi \sim 0.545$. Beyond that, a rough saturation was found in Ref. [51], and perhaps even a hint of nonmonotonicity. We do not find these latter trends intuitive, and they are likely not reliable since crystallization occurred in the simulations, more so with increasing packing fraction, and the simulation runs were short [51,52].

Other recent simulation studies of monodisperse hard sphere fluids [41,42] have only been performed in the lower density normal fluid regime. Our simulations results, those of Ref. [51], and the MV calculations are all in good agreement with each other and the data of Refs. [41,42] in this normal fluid regime; an explicit example of this can be seen in Fig. 7(b) where results down to $\phi = 0.45$ are shown. Finally,

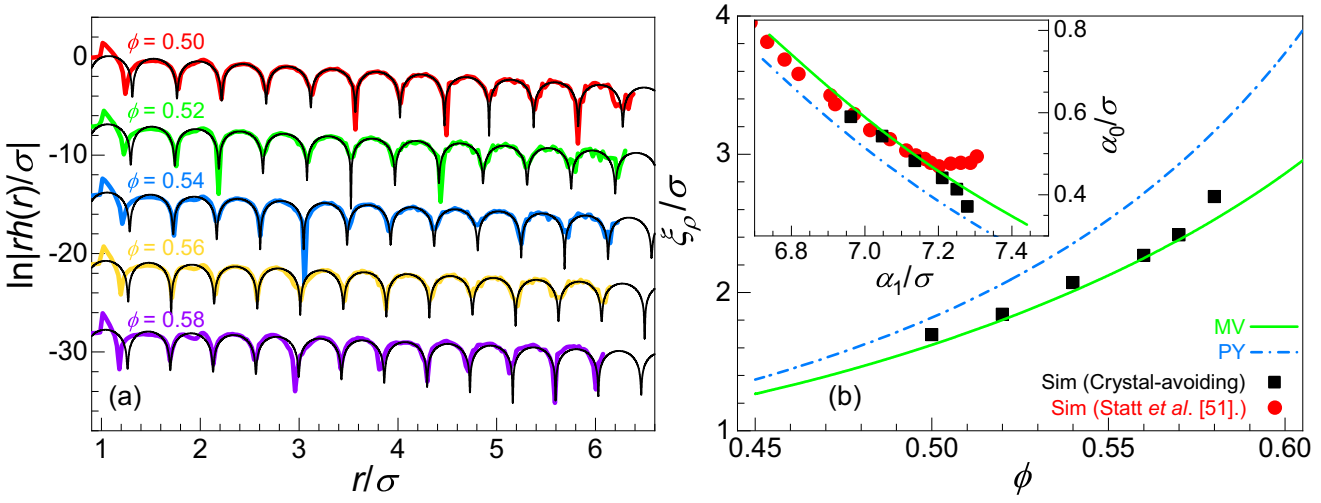

FIG. 7. (a) Plot of $\ln|rh(r)/\sigma|$ for metastable monodisperse hard spheres based on crystal-avoiding simulation method. The black curves are fits to Eq. (12). (b) Correlation length $\xi_\rho = \sigma/\alpha_0$ obtained from simulation compared with the predictions of OZ-PY and OZ-MV theories. Inset: comparison of the values of α_0 and α_1 in Eq. (12) determined from crystal-avoiding simulations, standard simulation methods [51], and the PY and MV approximations.

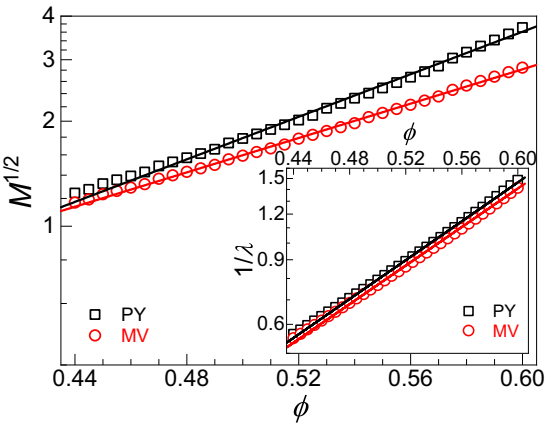

FIG. 8. Packing fraction dependence of the two density fluctuation correlation lengths deduced from $S(q)$ as defined in the text, as predicted based on the PY and MV closures. The lines in the main frame and inset are exponential fits with parameters listed in Table I.

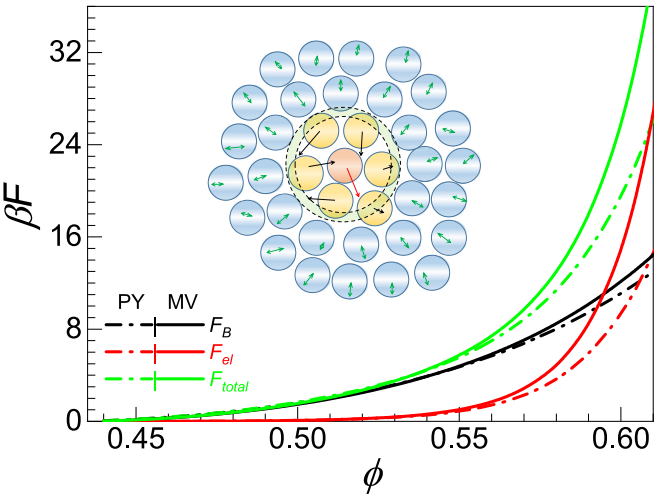

FIG. 9. Comparison of the local cage barrier (F_B), collective elastic barrier (F_{el}), and total dynamic barrier (F_{total}) of the activated relaxation ECNLE theory [16,36] based on $S(q)$ input computed using the PY (dash-dotted) and MV (solid) closure approximations. Inset: schematic of the conceptual elements of the ECNLE theory where the activated structural relaxation event is of a coupled local-nonlocal nature.

we note that experiments and other simulations up to a packing fraction of $\phi = 0.6$ [53] have studied various real-space correlation lengths, but these employed polydisperse systems and focused on locally favored structures and hence are not germane to our present work.

E. Fourier-space correlation length

We now study correlation lengths and other quantities that can be extracted from $S(q)$. As expected, we find (see Table I) that the exponential growth of the real-space correlation length and its associated B value agrees well with the behavior of $S_{\max}$ in Fig. 4. This connection between real- and Fourier-space is buttressed by extracting a correlation length from $S(q)$ in two ways. The first is from the full width at half height of the primary peak of the structure factor, λ from which we define a length scale as $l = \pi/\lambda$. The second is to quadratically expand $1/S(q)$ around its first peak at $q = q^*$ (a local Lorentzian approximation) thereby defining a correlation length Ψ:

$$S^{-1}(q) \approx S^{-1}(q^*)[1 + \Psi^2(q - q^*)^2]. \tag{13}$$

Using the exact relation $S^{-1}(q) = 1 - \rho C(q)$, the length scale in Eq. (13) is

$$\Psi = \sqrt{-\frac{1}{2}S(q^*)\left[\frac{d^2\rho C(q)}{dq^2}\right]_{q=q^*}}. \tag{14}$$

Figure 8 shows theoretical results for these length scales. Their exponential density dependences are nearly identical, and almost the same as the real-space analog ξ_ρ, with $B \sim 6$ to 7 (Table I). Based on the most accurate MV calculations, Table I suggests that to leading order these three length scales and $S_{\max}$ grow exponentially with packing fraction with a very similar B value.

Interestingly, the four local quantities discussed above all exhibit an exponential packing fraction dependence, as does the long wavelength thermodynamic quantity $1/S_0$. Based on MV theory, the value of B for the inverse dimensionless compressibility computed using the more accurate virial route is roughly twice that of the various correlation lengths extracted by analysis of finite length scale structural features. This suggests an interesting correlation between the density dependent growth of different metrics of static density correlations, with potentially significant dynamical implications. For example, if there is a deep connection between equilibrium properties and the alpha relaxation time in supercooled or overcompressed liquids, then our results suggest a type of degeneracy of interpretation with regard to the existence of *practical* empirical correlations between slow dynamics and thermodynamic and/or local structural order quantities based on density fluctuations. The elementary reason is that any function that varies exponentially with density when raised to *any* power remains of an exponential form. Moreover, if the dynamic barrier relevant to the alpha relaxation process is proportional to any of the aforementioned quantities (raised to any power), the corresponding relaxation time will empirically be a *double exponential* function of packing fraction. The above logic does not apply for other mathematical functions of density such as power laws or an exponential of a multiterm polynomial.

Concerning the quality of MV versus PY closure predictions, the former is significantly better for both thermodynamic properties and the real- and Fourier-space structure, $g(r)$ and $S(q)$. However, both closures predict that all five quantities in Table I grow exponentially with packing fraction to a good approximation. Quantitatively, the absolute value and increase with packing fraction of the three density correlations lengths and cage peak amplitude $S_{\max}$ are all larger for PY than for MV, reflecting the systematic difference between these two approximations. Though these differences may seem modest for these properties, they are manifested in significant differences for the EOS.

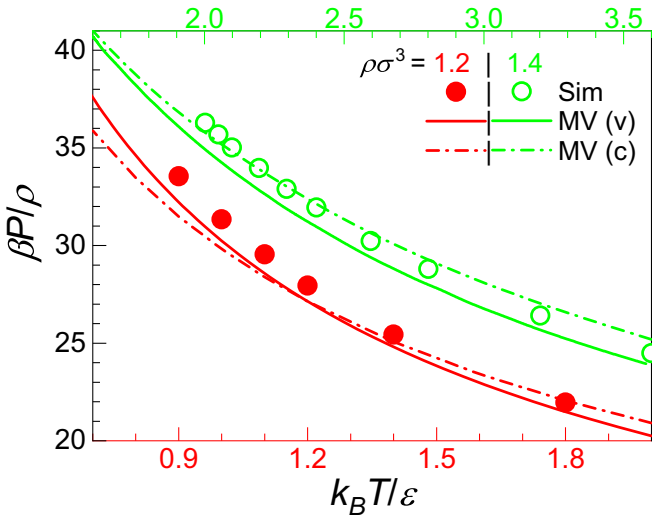

FIG. 10. Dimensionless pressure of WCA fluids in the metastable regime as a function of reduced temperature at reduced densities of $\rho\sigma^3 = 1.2$ (red) and 1.4 (green) based on MV virial (solid) and compressibility (dash-dotted) route calculations. Simulation data are the red and green circles; note the lower x-axis is for the solid circles and a reduced density of 1.2, while the upper x-axis is for the open circles and a reduced density of 1.4.

F. Dynamic implications

We emphasize that a static length scale associated with a two-point correlation function that grows with packing fraction is also relevant to isobaric experiments on supercooled liquids where, typically, density increases with cooling. Moreover, isobaric experiments on a variety of fragile glass-forming liquids find the primary wide angle peak of $S(q)$ grows significantly with cooling, and suggestions for its connection to glassy dynamics have been proposed [54,55]. Since glassy dynamics is known to be very sensitive to small changes of thermodynamic state and structure, the predictions of microscopic theories of activated relaxation are expected to be nontrivially sensitive to using PY versus MV structural input. Though this topic is beyond the scope of this article, it is a primary motivation for our present work. This motivates our presentation in Fig. 9 of an illustrative calculation of how the local cage, collective elastic, and total dynamic barriers in the units of thermal energy evolve with packing fraction for a hard sphere fluid based on ECNLE theory [16]; we note that the mean structural relaxation time scales as the exponential of $\beta F_{\rm total}$. In the present context, the relevant point is ECNLE theory requires *only* $S(q)$ as input, which we have shown in this article is significantly more accurately predicted in the metastable regime based on the MV closure than its PY analog. The differences in the barriers based on the structural input from the two closures seen in Fig. 9 are significant, and their consequences will be studied in a future publication.

IV. WCA FLUID

We have also performed OZ-MV calculations for supercooled metastable states of the WCA fluid and compared the results with our crystal-avoiding simulations. The WCA potential is defined as [1]:

$$u_{\rm WCA}(r) = \begin{cases} 4\epsilon\left[\left(\frac{\sigma}{r}\right)^{12} - \left(\frac{\sigma}{r}\right)^{6}\right] + \epsilon, & r \leqslant 2^{1/6}\sigma \\ 0, & r > 2^{1/6}\sigma \end{cases}, \quad (15)$$

where ϵ is the energy scale and σ the nominal length scale. The reduced density and temperature are defined as $\rho\sigma^3$ and $k_{\rm B}T/\epsilon$, respectively, where $k_{\rm B}$ is the Boltzmann constant. Here we employ for simplicity the same values of a_1 and a_2 in Eq. (4) which were optimized for hard spheres. Hence, we expect the theoretical results will not be as accurate for the WCA fluid as found for hard spheres. We emphasize that all the simulation results in Figs. 10–12 are in the metastable low temperature and high density regime, in contrast to our prior brief study [24] of the equation of state of the WCA fluid in the normal fluid regime.

Figure 10 shows the dimensionless EOS as a function of reduced temperature for the two high reduced densities of 1.2 and 1.4. Rather good thermodynamic consistency and agreement with simulation is found, albeit not as quantitatively

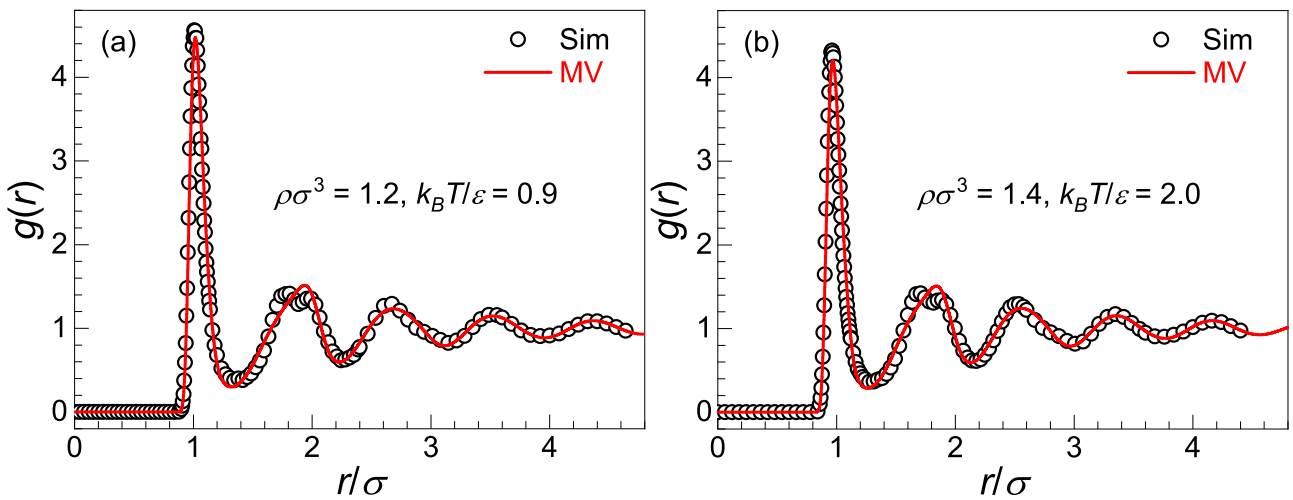

FIG. 11. Pair correlation function of WCA fluids in the metastable regime at dimensionless densities and temperatures of (a) $\rho\sigma^3 = 1.2$ and $k_{\rm B}T/\epsilon = 0.9$, and (b) $\rho\sigma^3 = 1.4$ and $k_{\rm B}T/\epsilon = 2.0$. Solid curves are the MV theory and open circles the simulation data.

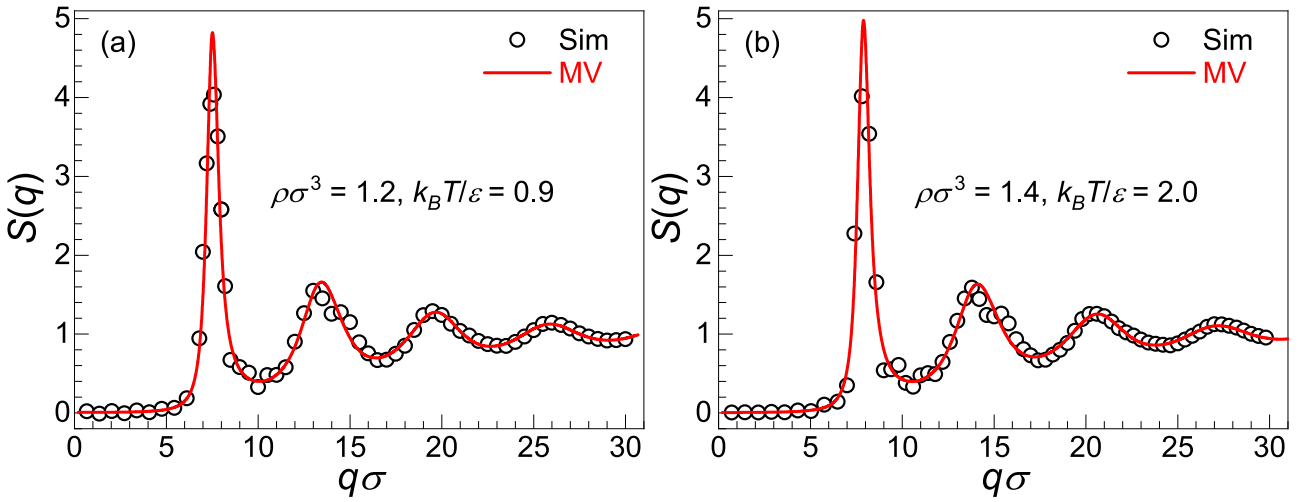

FIG. 12. Structure factor as a function of dimensionless wave vector of WCA fluids in the metastable regime for dimensionless densities and temperatures of (a) $\rho\sigma^3 = 1.2$ and $k_BT/\epsilon = 0.9$, and (b) $\rho\sigma^3 = 1.4$ and $k_BT/\epsilon = 2.0$. Solid curves are the MV theory and open circles the simulation data.

good as found for hard spheres. Overall, the virial route-based results are modestly better than their compressibility route analogs, a conclusion that also applies to hard spheres.

Figures 11 and 12 show representative structural results in real- and Fourier-space, respectively. For each density, only the results for the lowest temperature studied is presented since it provides the most incisive test of theory. The predicted $g(r)$'s in Fig. 11 are in excellent accord with simulation, with (again) the exception of no weakly split second peak. The analogous structure factors in Fig. 12 are also quite accurate, albeit the intensity of the first peak is overpredicted. The latter deviation is much smaller at higher temperatures (not shown), and modestly worse at higher density. As expected, the theoretical predictions for $S(q)$ are not as good as we found for hard spheres.

V. SUMMARY

We have applied OZ integral equation theory with the PY and MV closures to study the equilibrium structural and thermodynamic properties of monodisperse hard sphere and WCA fluids under density and temperature conditions where the system is overcompressed or supercooled (metastable relative to crystallization). The theoretical results were compared to our present crystal-avoiding simulations. This is a comprehensive application of MV-OZ theory to study thermodynamic properties and real- and Fourier-space structure and correlation lengths of *metastable* hard sphere and WCA fluids.

As found previously [24], for the hard sphere fluid $g(r)$ the MV results at small distances (including the contact value) are much better than their PY analog, and also in good absolute agreement with simulation. The MV virial route produces excellent results for the EOS for all packing fractions. MV-based results for the static structure factor and various local and long wavelength measures of density fluctuations associated with the real- and Fourier-space pair correlations were obtained. Overall the MV-based OZ theory performs very well, and is far more accurate and thermodynamically self-consistent than the analogous PY-based approach.

Rather remarkably, two measures of density fluctuation order parameter amplitude (on the cage scale and $q = 0$) and density correlation lengths extracted in three distinct manners are all predicted to grow in an exponential manner with packing fraction over the metastable regime studied. The established behaviors are directly relevant to microscopic theories (e.g., MCT [14,56], ECNLE theory [6,16]) that relate dynamical constraints to structural pair correlations, an issue that will be explored in a future article. Our present simulations have also revealed that the real-space density correlation length continues to grow up to the highest packing fraction (0.58) for which we are able to achieve full equilibration.

We studied several high density and low temperature states of the WCA fluid in the metastable regime. The MV-based theory of structure and thermodynamics is again quite accurate, though not as quantitatively good as for hard spheres. This is unsurprising since no attempt was made to adjust the two parameters of the MV closure for the WCA potential. This is an avenue for future work, not only for the WCA potential, but also other soft matter systems characterized by repulsive interactions of variable softness and spatial range.

ACKNOWLEDGMENTS

Y.Z. and K.S.S. acknowledge support from the U.S. Department of Energy, Office of Science, Basic Energy Sciences, Materials Sciences and Engineering Division. B.M. and K.S.S. acknowledge support from DOE-BES under Grant No. DE-FG02-07ER46471 administered through the Materials Research Laboratory at UIUC.

[1] J.-P. Hansen and I. R. McDonald, *Theory of Simple Liquids* (Elsevier, Amsterdam, 2006).

[2] *Theory and Simulation of Hard-Sphere Fluids and Related Systems*, edited by Á. Mulero, Lecture Notes in Physics 753 (Springer, Berlin, Heidelberg, 2008).

[3] P. N. Pusey, E. Zaccarelli, C. Valeriani, E. Sanz, W. C. K. Poon, and M. E. Cates, Hard spheres: Crystallization and glass formation, Philos. Trans. R. Soc. A **367**, 4993 (2009).

[4] A. R. Kansal, S. Torquato, and F. H. Stillinger, Diversity of order and densities in jammed hard-particle packings, Phys. Rev. E **66**, 041109 (2002).

[5] M. D. Rintoul and S. Torquato, Computer simulations of dense hard-sphere systems, J. Chem. Phys. **105**, 9258 (1996).

[6] S. Mirigian and K. S. Schweizer, Elastically cooperative activated barrier hopping theory of relaxation in viscous fluids. I. General formulation and application to hard sphere fluids, J. Chem. Phys. **140**, 194506 (2014).

[7] J. K. Percus and G. J. Yevick, Analysis of classical statistical mechanics by means of collective coordinates, Phys. Rev. **110**, 1 (1958).

[8] M. Ozawa and L. Berthier, Does the configurational entropy of polydisperse particles exist? J. Chem. Phys. **146**, 014502 (2017).

[9] G. L. Hunter and E. R. Weeks, The physics of the colloidal glass transition, Rep. Prog. Phys. **75**, 066501 (2012).

[10] W. Kob and H. C. Andersen, Testing mode-coupling theory for a supercooled binary Lennard-Jones mixture I: The van Hove correlation function, Phys. Rev. E **51**, 4626 (1995).

[11] L. Berthier, D. Coslovich, A. Ninarello, and M. Ozawa, Equilibrium Sampling of Hard Spheres up to the Jamming Density and Beyond, Phys. Rev. Lett. **116**, 238002 (2016).

[12] Y. Zhou and S. T. Milner, T1 process and dynamics in glass-forming hard-sphere liquids, Soft Matter **11**, 2700 (2015).

[13] Y. Zhou and S. T. Milner, A geometrical criterion for glass transition in soft-sphere fluids, Soft Matter **14**, 7075 (2018).

[14] W. Götze, *Complex Dynamics of Glass-Forming Liquids: A Mode-Coupling Theory* (Oxford University Press, Oxford, 2009).

[15] K. S. Schweizer, Derivation of a microscopic theory of barriers and activated hopping transport in glassy liquids and suspensions, J. Chem. Phys. **123**, 244501 (2005).

[16] S. Mirigian and K. S. Schweizer, Elastically cooperative activated barrier hopping theory of relaxation in viscous fluids. II. Thermal liquids, J. Chem. Phys. **140**, 194507 (2014).

[17] T. R. Kirkpatrick, D. Thirumalai, and P. G. Wolynes, Scaling concepts for the dynamics of viscous liquids near an ideal glassy state, Phys. Rev. A **40**, 1045 (1989).

[18] V. Lubchenko and P. G. Wolynes, Theory of structural glasses and supercooled liquids, Annu. Rev. Phys. Chem. **58**, 235 (2007).

[19] G. Parisi and F. Zamponi, Mean-field theory of hard sphere glasses and jamming, Rev. Mod. Phys. **82**, 789 (2010).

[20] L. Verlet, Integral equations for classical fluids: I. The hard sphere case, Mol. Phys. **41**, 183 (1980).

[21] L. Verlet, Integral equations for classical fluids: II. Hard spheres again, Mol. Phys. **42**, 1291 (1981).

[22] M. Kinoshita, Interaction between surfaces with solvophobicity or solvophilicity immersed in solvent: Effects due to addition of solvophobic or solvophilic solute, J. Chem. Phys. **118**, 8969 (2003).

[23] J. A. Perera-Burgos, J. M. Méndez-Alcaraz, G. Pérez-Ángel, and R. Castañeda-Priego, Assessment of the micro-structure and depletion potentials in two-dimensional binary mixtures of additive hard-disks, J. Chem. Phys. **145**, 104905 (2016).

[24] Y. Zhou and K. S. Schweizer, Local structure, thermodynamics, and phase behavior of asymmetric particle mixtures: Comparison between integral equation theories and simulation, J. Chem. Phys. **150**, 214902 (2019).

[25] A. Donev, F. H. Stillinger, and S. Torquato, Unexpected Density Fluctuations in Jammed Disordered Sphere Packings, Phys. Rev. Lett. **95**, 090604 (2005).

[26] D. Chandler, J. D. Weeks, and H. C. Andersen, Van der Waals picture of liquids, solids, and phase transformations, Science **220**, 787 (1983).

[27] R. Evans, Density functionals in the theory of nonuniform fluids, in *Fundamentals of Inhomogeneous Fluids*, edited by D. Henderson (Marcel Dekker, New York, 1992), pp. 85–176.

[28] R. Evans, The nature of the liquid-vapour interface and other topics in the statistical mechanics of non-uniform, classical fluids, Adv. Phys. **28**, 143 (1979).

[29] T. Biben and J.-P. Hansen, Phase Separation of Asymmetric Binary Hard-Sphere Fluids, Phys. Rev. Lett. **66**, 2215 (1991).

[30] M. Dijkstra, R. van Roij, and R. Evans, Phase Behavior and Structure of Binary Hard-Sphere Mixtures, Phys. Rev. Lett. **81**, 2268 (1998).

[31] L. M. Hall and K. S. Schweizer, Many body effects on the phase separation and structure of dense polymer-particle melts, J. Chem. Phys. **128**, 234901 (2008).

[32] J. B. Hooper and K. S. Schweizer, Contact aggregation, bridging, and steric stabilization in dense polymer−particle mixtures, Macromolecules **38**, 8858 (2005).

[33] K. S. Schweizer and E. J. Saltzman, Activated hopping, barrier fluctuations, and heterogeneity in glassy suspensions and liquids, J. Phys. Chem. B **108**, 19729 (2004).

[34] S. Ciarella, R. A. Biezemans, and L. M. C. Janssen, Understanding, predicting, and tuning the fragility of vitrimeric polymers, Proc. Natl. Acad. Sci. USA **116**, 25013 (2019).

[35] T. Sentjabrskaja, A. R. Jacob, S. U. Egelhaaf, G. Petekidis, T. Voigtmann, and M. Laurati, Binary colloidal glasses: Linear viscoelasticity and its link to the microscopic structure and dynamics, Soft Matter **15**, 2232 (2019).

[36] S. Mirigian and K. S. Schweizer, Unified theory of activated relaxation in liquids over 14 decades in time, J. Phys. Chem. Lett. **4**, 3648 (2013).

[37] A. Ghosh and K. S. Schweizer, Microscopic theory of the influence of strong attractive forces on the activated dynamics of dense glass and gel forming fluids, J. Chem. Phys. **151**, 244502 (2019).

[38] E. D. Cubuk, S. S. Schoenholz, J. M. Rieser, B. D. Malone, J. Rottler, D. J. Durian, E. Kaxiras, and A. J. Liu, Identifying Structural Flow Defects in Disordered Solids Using Machine-Learning Methods, Phys. Rev. Lett. **114**, 108001 (2015).

[39] F. P. Landes, G. Biroli, O. Dauchot, A. J. Liu, and D. R. Reichman, Attractive versus truncated repulsive supercooled liquids: The dynamics is encoded in the pair correlation function, Phys. Rev. E **101**, 010602(R) (2020).

[40] D. Henderson and E. W. Grundke, Direct correlation function: Hard sphere fluid, J. Chem. Phys. **63**, 601 (1975).

[41] S. Pieprzyk, A. C. Brańka, and D. M. Heyes, Representation of the direct correlation function of the hard-sphere fluid, Phys. Rev. E **95**, 062104 (2017).
[42] S. Pieprzyk, A. C. Brańka, S. B. Yuste, A. Santos, and M. L. De Haro, Structural properties of additive binary hard-sphere mixtures, Phys. Rev. E **101**, 012117 (2020).
[43] D. A. McQuarrie, *Statistical Mechanics* (Harper & Row, New York, 1976).
[44] K. S. Schweizer and E. J. Saltzman, Entropic barriers, activated hopping, and the glass transition in colloidal suspensions, J. Chem. Phys. **119**, 1181 (2003).
[45] K. S. Schweizer and G. Yatsenko, Collisions, caging, thermodynamics, and jamming in the barrier hopping theory of glassy hard sphere fluids, J. Chem. Phys. **127**, 164505 (2007).
[46] M. Fuchs, MCT results for a simple liquid at the glass transition, Transp. Theory Stat. Phys. **24**, 855 (1995).
[47] R. Zwanzig, *Nonequilibrium Statistical Mechanics* (Oxford University Press, Oxford, 2001).
[48] T. M. Truskett, S. Torquato, S. Sastry, P. G. Debenedetti, and F. H. Stillinger, Structural precursor to freezing in the hard-disk and hard-sphere systems, Phys. Rev. E **58**, 3083 (1998).
[49] S. Mirigian and K. S. Schweizer, Dynamical theory of segmental relaxation and emergent elasticity in supercooled polymer melts, Macromolecules **48**, 1901 (2015).
[50] A. C. Brańka and D. M. Heyes, Pair correlation function of soft-sphere fluids, J. Chem. Phys. **134**, 64115 (2011).
[51] A. Statt, R. Pinchaipat, F. Turci, R. Evans, and C. P. Royall, Direct observation in 3D of structural crossover in binary hard sphere mixtures, J. Chem. Phys. **144**, 144506 (2016).
[52] A. Statt, private communication (2020).
[53] J. E. Hallett, F. Turci, and C. P. Royall, Local structure in deeply supercooled liquids exhibits growing lengthscales and dynamical correlations, Nat. Commun. **9**, 3272 (2018).
[54] N. A. Mauro, M. Blodgett, M. L. Johnson, A. J. Vogt, and K. F. Kelton, A structural signature of liquid fragility, Nat. Commun. **5**, 4616 (2014).
[55] D. N. Voylov, P. J. Griffin, B. Mercado, J. K. Keum, M. Nakanishi, V. N. Novikov, and A. P. Sokolov, Correlation between temperature variations of static and dynamic properties in glass-forming liquids, Phys. Rev. E **94**, 060603(R) (2016).
[56] D. R. Reichman and P. Charbonneau, Mode-coupling theory, J. Stat. Mech. (2005) P05013.